Determination of absorption cross-section of Si nanocrystals by two independent methods based on either absorption or luminescence

J. Valenta,[1,a)] M. Greben,[1] Z. Remeš,[2] S. Gutsch,[3] D. Hiller,[3] and M. Zacharias[3]
[1]*Department of Chemical Physics and Optics, Faculty of Mathematics and Physics, Charles University, Ke Karlovu 3, 121 16 Prague 2, Czechia*
[2]*Institute of Physics, Academy of Sciences of the Czech Republic, Cukrovarnická 10, Prague 6, Czechia*
[3]*Faculty of Engineering, IMTEK, Albert-Ludwigs-University Freiburg, Georges-Köhler-Allee 103, 79110 Freiburg, Germany*

(Received 25 September 2015; accepted 28 December 2015; published online 11 January 2016)

Absorption cross-section (ACS) of silicon nanocrystals (SiNCs) is determined via two completely independent approaches: (i) Excitation-intensity-dependent photoluminescence (PL) kinetics under modulated (long square pulses) pumping and (ii) absorbance measured by the photothermal deflection spectroscopy combined with morphology information obtained by the high-resolution transmission electron microscopy. This unique comparison reveals consistent ACS values around 10^{-15} cm^2 for violet excitation of SiNCs of about 3–5 nm in diameter and this value is comparable to most of direct band-gap semiconductor nanocrystals; however, it decreases steeply towards longer wavelengths. Moreover, we analyze the PL-modulation technique in detail and propose an improved experimental procedure which enables simpler implementation of this method to determine ACS of various (nano)materials in both solid and liquid states. © *2016 AIP Publishing LLC*. [http://dx.doi.org/10.1063/1.4939699]

Optical properties of nanostructured materials can significantly differ from the respective bulk materials. Numerous reports showed optical changes like the blue shift of the absorption edge due to the band gap opening and improvement of luminescence efficiency with decreasing size of nanostructures.[1] In case of optically excited nanomaterials (useable as detectors, absorbers in solar cells,[2] or as luminescent labels[3]), a crucial optical property is the ability to efficiently absorb light—most often described by the absorption cross-section (ACS) σ of a nanoobject (nanocrystal (NC), nanowire, etc.). Typical values of σ for direct band gap semiconductor NCs are between[4] 10^{-14} and 10^{-16} cm^2. Very interesting effects can take place for indirect band gap semiconductors, where an increase of absorption probability is expected as a result of strong spatial localization of electron and hole wavefunctions leading to their delocalization in k-space and possible quasi-direct transitions. In spite of this well known prediction, systematical investigation of ACS in the most important semiconductor, i.e., Si, was not reported yet; one of the reasons could be experimental difficulties. In this letter, we describe a modified photoluminescence (PL) modulation technique for the determination of ACS in SiNCs. Direct comparison of ACS values from PL with completely independent absorption method enables to demonstrate advantages and disadvantages of both techniques. Knowledge of effective ACS in ensembles of NCs is crucial for design of nanostructured absorbers for solar cells, detectors, and other applications.

The investigated samples were deposited by the plasma-enhanced chemical vapor deposition (PE-CVD) as alternating layers of silicon-rich silicon oxynitride (SRON) SiO_xN_y and stoichiometric silicon dioxide SiO_2 (2 or 2.2 nm thick) on fused silica substrates. On top and below the 40-bilayer stack, 10-nm layers of SiO_2 were deposited as the buffer and capping layers, respectively. The samples were consequently annealed in a quartz tube furnace at 1150 °C for 1 h in high purity N_2 in order to form SiNCs and then passivated by annealing in H_2 at 500 °C. The main parameters of the investigated samples are given in Table I. Further details of the sample preparation are given in our recent paper.[5] The shape and size distribution of Si NCs were studied by preparing special monolayer (ML)-SRON samples directly on transmission electron microscopy (TEM) grids that were consequently studied by the high-resolution energy-filtered TEM (EF-TEM).[6] For samples W3 to W6, we found[6] the Si NCs areal density between 3.8 and 2.4×10^{-12} cm^{-2} (see Table I), but the narrower SRON layers give no clear EF-TEM images of SiNCs most probably due to imperfect phase separation or low EF-TEM contrast. Therefore, the density of NCs for samples W1 and W2 was estimated by extrapolation.

Absorbance of the studied samples was obtained by the *photothermal deflection spectroscopy* (PDS)[7] which detects heating waves produced by dissipation of modulated incident light. It is able to detect absorbance down to 10^{-5}. PL experiments were performed under excitation by a 405-nm diode laser whose beam was modulated using a quartz acousto-optic cell. The resulting square-shaped pulses have the duty cycle of 40%, the repetition rate of 900 Hz, and the edge switching time of about 100 ns. The laser is coupled to a home made micro-spectroscopy set-up with an inverted microscope in the epifluorescence configuration. There are two detection branches for visible (VIS) and near-infrared (NIR) spectral regions, each one composed of an imaging spectrometer (Acton SpectraPro SP-2358i and SP-2558i, respectively) and a photomultiplier (PMT) for time-resolved

a)Author to whom correspondence should be addressed. Electronic mail: jan.valenta@mff.cuni.cz.

TABLE I. Description of the sample parameters.

Label	SiO_xN_y thick. (nm)	SiO_2 thick. (nm)	Stoichiometry x-value	Single layer NC areal density (10^{12} cm^{-2})	PL QY (exc. 405 nm)
W1	1.5	2.0	1.0	Estim. 5 ± 0.5	0.14 ± 0.03
W2	2.5	2.0	1.0	Estim. 4.4 ± 0.4	0.18 ± 0.02
W3	3.5	2.0	1.0	3.8 ± 0.3	0.21 ± 0.02
W4	4.5	2.0	1.0	3.4 ± 0.3	0.20 ± 0.02
W5	4.5	1.6	0.93	2.43 ± 0.05	0.18 ± 0.01
W6	4.5	2.2	0.93	2.43 ± 0.05	0.19 ± 0.02

PL detection (Hamamatsu H11526-20-NF and H10330A-45, respectively, for VIS and NIR). Pulses from PMTs are detected by two multichannel counting cards (Becker-Hickl, MSA-300). The significant advantage of the imaging micro-PL set-up for the PL-modulation ACS method is the good control of the excitation spot size and the signal collection area which enable quite precise determination of excitation photon flux. More details on the set-up can be found in our recent paper.[8]

The first approach to determine ACS is based on measuring the pumping intensity dependence of the time-resolved PL response to the square-modulated excitation. The PL from an ensemble of NCs can be well described by a set of three differential equations, when only three possible states of a NC are considered: ground state, single and double excited state (i.e., one or two electron-hole pairs (excitons) in a NC) with the corresponding occupations N_0, N_1, and N_2

$$\frac{dN_0}{dt} = -N_0 I_{ex}\sigma + \frac{N_1}{\tau_{PL}}, \tag{1}$$

$$\frac{dN_1}{dt} = N_0 I_{ex}\sigma - N_1 I_{ex}\sigma - \frac{N_1}{\tau_{PL}} + \frac{N_2}{\tau_A}, \tag{2}$$

$$\frac{dN_2}{dt} = N_1 I_{ex}\sigma - \frac{N_2}{\tau_A}. \tag{3}$$

Here, I_{ex} is excitation intensity expressed in photon flux (photons per second per cm^2), and τ_{PL} and τ_A are luminescence and Auger lifetime, respectively. The total number of luminescing NCs is $N_T = N_0 + N_1 + N_2$. Any higher excited state is not considered supposing that the Auger quenching of doubly excited population is very fast and efficient (τ_A is reported to be in the ns-range or shorter[9]). A similar description presented by Kovalev *et al.*[10] considered erroneously the radiative lifetime τ_r instead of the correct τ_{PL} which contains both radiative and non-radiative lifetimes ($1/\tau_{PL} = 1/\tau_r + 1/\tau_{nr}$). The use of the same σ for absorption from both the ground state and the single-excited state may be substantiated by the high density of states in SiNCs.[11]

The steady state (i.e., all $dN/dt = 0$) PL intensity at moderate excitation ($N_T \approx N_0$) should, obviously, be a linear function of excitation power. From Eq. (2), we obtain $N_1 = N_T I_{ex}\sigma\tau_{PL}$ and then PL intensity reads as

$$I_{PL} = \frac{N_1}{\tau_r} = N_T I_{ex}\sigma\,\frac{\tau_{PL}}{\tau_r} = N_T I_{ex}\sigma\eta, \tag{4}$$

where $\eta = \tau_{PL}/\tau_r$ is the PL quantum yield (QY).[12] So, the slope of the $I_{PL}(I_{ex})$ linear dependence is $N_T\sigma\eta$ and σ can be determined if the PL QY and density of NCs are known. However, one has also to know the scale of the intensity axis, i.e., the absolute spectral calibration—relation between the detected signal (e.g., in counts per second) and the number of emitted photons. Such an absolute calibration of a spectrometer set-up is complicated, therefore some authors exploited PL intensity saturation instead.[10] Under strong excitation, the assumption that $N_T \approx N_0$ is no more valid. Considering fast Auger quenching, N_2 is negligible and the PL power saturation curve is described by

$$I_{PL} = \frac{N_1}{\tau_r} = \frac{N_T I_{ex}\sigma\eta}{1 + I_{ex}\sigma\tau_{PL}}. \tag{5}$$

The deviation from linear dependence is described by the denominator, namely, the factor $\sigma\tau_{PL}$. When the PL decay time τ_{PL} is determined from a separate experiment, σ can be obtained by fitting of the PL power saturation. In Fig. 2(a), we present an example of the saturation fit, which works well for the beginning of saturation but deviates significantly for stronger pumping. The non-complete saturation of PL of SiNCs under cw excitation seems to be a general effect that we studied in detail and will be published separately. Anyway, PL saturation in our multilayer samples cannot be satisfactorily fitted by Eq. (5) and attempts to do so (see Fig. 2(a)) give quite low values of σ (similar as obtained by Garcia *et al.*[13] using the same method). Therefore, we turned to the PL modulation technique.

The PL onset after switching on a constant excitation is described by Eq. (2), which has the following solution:

$$\begin{aligned} I_{PL}(t) = \frac{N_1(t)}{\tau_r} &= N_T I_{ex}\sigma\eta\left\{1 - \exp\left[-t\left(\frac{1}{\tau_{PL}} + I_{ex}\sigma\right)\right]\right\} \\ &= I_{PL}^{cw}\left(1 - e^{-t/\tau_{ON}}\right). \end{aligned} \tag{6}$$

This means that the PL intensity exponentially approaches the equilibrium value with characteristic time τ_{ON} which is a function of excitation photon flow

$$\frac{1}{\tau_{ON}} = \frac{1}{\tau_{PL}} + I_{ex}\sigma. \tag{7}$$

Consequently, the ACS can be directly obtained as the slope of pumping power dependence of the ON-OFF differential rate ($1/\tau_{ON} - 1/\tau_{PL}$) which should be a linear function of excitation power. Such approach was exploited in various studies, but its application limits were not described yet. Most importantly, Eq. (7) is valid only within the limited range of excitation power close to the PL saturation; for low I_{ex}, the values of τ_{ON} and τ_{PL} must be equal and for high pumping

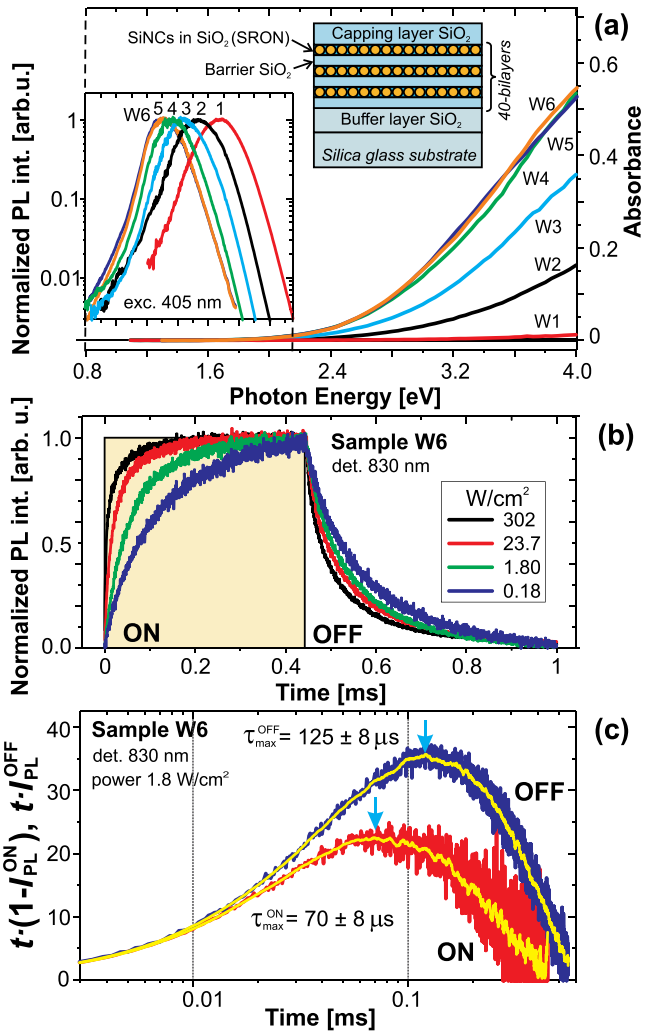

FIG. 1. (a) Absorbance (right) and PL (left) spectra of the investigated samples. The inset illustrates the multilayer sample structure. (b) Time-resolved PL signal excited by the square pulses with power density ranging from 0.18 to 302 W/cm^2. (c) Normalized PL onset and decay signals multiplied by time which represents density of decay rates (yellow lines are smoothed curves obtained by the adjacent-point averaging). The peak positions reveal the dominant time constants.

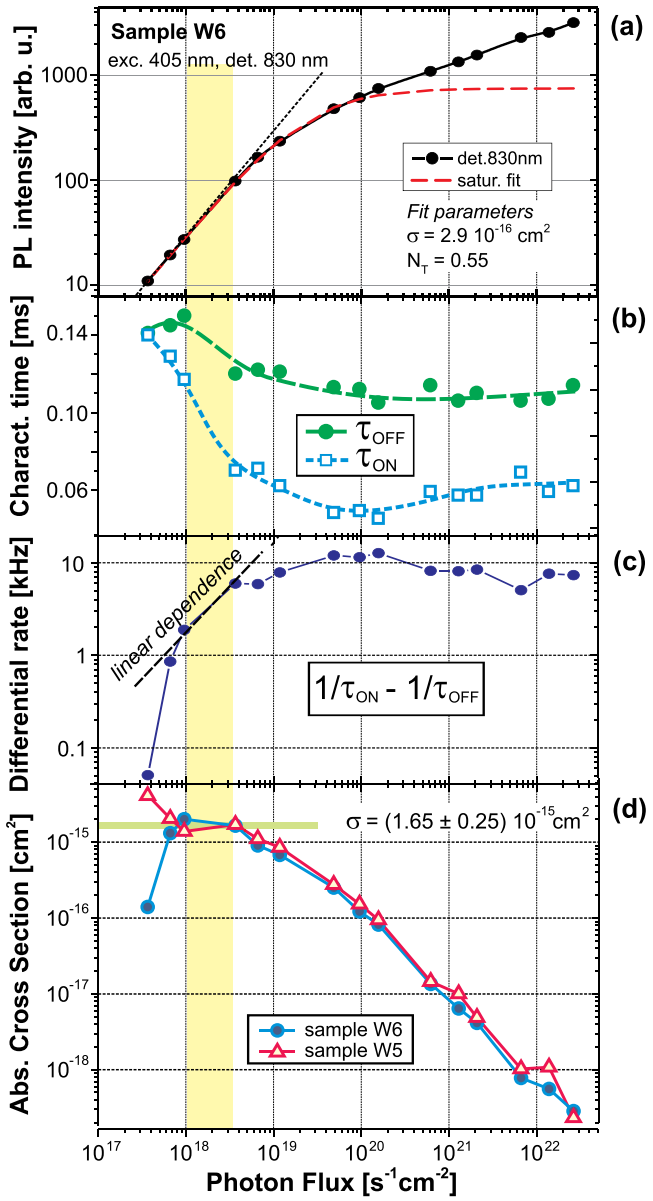

FIG. 2. (a) PL intensity under cw excitation as function of excitation photon flux. The dashed line is the fit using the PL saturation model described by Eq. (5), which deviates significantly from experimental points for strong excitation and gives too low ACS value (about 6 times). (b) The extracted ON and OFF characteristic times and (c) the resulting differential rates. (d) Final ACS obtained from PL-modulation in the samples W5 and W6.

Eq. (6) is no more valid as η becomes power dependent and the population N_2 is non-negligible.

Time-resolved PL traces were measured for various wavelengths (with step of 40 nm) and excitation power varied by five orders of magnitude around the PL saturation level (which is usually ~1 W/cm^2). Fig. 1(b) presents several PL time-traces for the sample W6 detected at 830 nm and normalized to the same peak intensity. For each trace, the peak and background PL signal is retrieved; the trace is normalized and then the major task is to find the representative characteristic times for the PL onset and decay. The problem, however, is that none part of the PL time evolution can be described by a single exponential function. It is well known that the PL decay in SiNCs is most often following the stretch exponential function[14] $I_{PL} = I_0 \exp[-(t/\tau)^{\beta}]$, but sometimes a more complicated function is needed. We tested several approaches for finding the dominant characteristic time and finally adopted the approach described by Higashi and Kastner[15] and recently applied to SiNCs by Hartel *et al.*[16] The method is based on the fact that the function $t \cdot I_{PL}(t)$ (PL decay signal multiplied by the delay time) is revealing a distribution of delay times. Then, the peak of this function can be taken as the dominant decay time of the distribution. More precise treatment must be done using the Laplace transformation but the method of Higashi and Kastner is precise enough and its big advantage is an easy algorithmization. In this paper, we determine τ of both onset and decay as maxima of the smoothed normalized functions $t \cdot (1 - I_{PL}{}^{ON})$ and $t \cdot I_{PL}{}^{OFF}$, see Fig. 1(c) for an example.

The power dependence of PL amplitude and characteristic times τ_{ON}, τ_{OFF} for PL at 830 nm from sample W6 are plotted in Figs. 2(a) and 2(b), respectively. As expected, both times are roughly equal at low excitation and then τ_{ON} decreases faster than τ_{OFF} when approaching PL saturation. In consequence, the resulting differential rate $1/\tau_{ON} - 1/\tau_{OFF}$

(Fig. 2(c)) is noisy at low excitation, almost constant for strong excitation above the saturation level, while the intermediate region of linear power dependence is surprisingly narrow at the toe of PL deviation from a linear dependence. This is the region where the above described model is valid and the ACS can be determined (Fig. 2(d)).

The spectral dependence of ACS was investigated for samples W1 to W4 over a broad range of emission wavelengths. Fig. 3(a) shows that ACS is increasing with the emission wavelength approaching the bulk Si band gap. Similar ACS spectra were obtained by Kovalev *et al.*[10] for porous Si and by Priolo *et al.*[22] for CVD grown SiNCs in oxide. By definition, ACS is related only to the absorption wavelength and should not depend on emission wavelength. The apparent emission-wavelength dependence is an effect of inhomogeneous broadening caused by significant size distribution of SiNCs within each sample. If we consider that ACS is a product of density of states and the transition oscillator strength only, where the former is increasing and the latter decreasing[17] with increasing NC size, then the effect of density of states seems to be stronger inducing ACS growth with SiNC size.[13] One can expect that for independent and well separated NCs, both ACS values and PL emission peak positions depend only on the NC size. But in various NC ensembles, the environment of NCs (matrix with other NCs) is changing which leads to modification of ACS. Indeed, we observe this effect (Fig. 3) especially for SiNC multilayers with SRON thickness below 3 nm (samples W1 and W2).

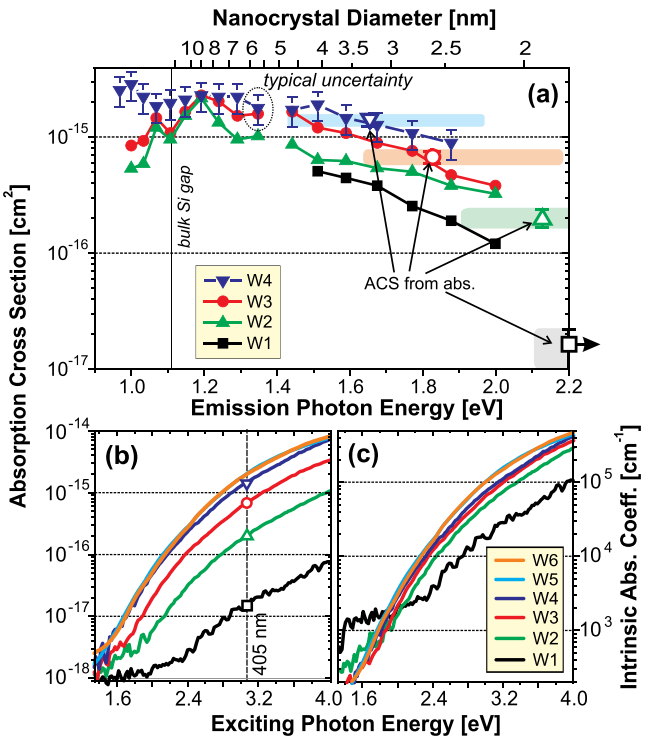

FIG. 3. (a) ACS determined via PL-modulation plotted as function of emission photon energy for samples W1 to W4. Estimated uncertainty (about 28%) is shown only for the sample W4). The upper scale is the NC diameter calculated according to Luo *et al.* Open symbols show ACS values obtained via absorption at 405 nm and plotted here at position of the mean NC size with indicated halfwidth of the size distribution (light rectangles). (b) ACS spectra calculated from absorbance and morphology data. (c) ACS spectra normalized to the mean NC volume.

Based on the presented analysis, we propose the following key points for implementation of the PL-modulation method to reveal ACS: (i) Determine the shape of PL power-saturation (for each studied wavelength) and find the appropriate power range for the time-resolved PL experiments; (ii) measure both onset and decay times of PL for excitation power varied within the defined range; (iii) calculate the differential rate and then ACS as a function of excitation power, and (iv) take the final ACS value from the region of constant power dependence or, if hardly observed, from the region around the PL-saturation onset.

Now we are going to compare the PL modulation results with the independent determination of ACS from absorbance A (logarithm of the ratio of incident to transmitted light power corrected for reflection and scattering losses, here we use the natural logarithm labeled A_e)[18] and the knowledge of NC density using this definition (applicable to optically thin samples)

$$A_e = \alpha d = \varepsilon c_M d = \sigma c_V d = \sigma c_A, \tag{8}$$

where α and ε are absorption and extinction coefficient, respectively. c_M, c_V, and c_A are the molar concentration, volume concentration, and area density, respectively, of absorbing NCs as seen by the incident wave.[19] The ACS spectra obtained from the absorbance and the morphology data (Table I) using Eq. (8) are plotted in Fig. 3(b). ACS values are monotonously increasing with absorbed photon energy and decreasing with the mean size of NCs. The latter effect can be due to decreasing volume of absorbing SiNCs; therefore, we present ACS divided by the NC volume (this quantity is called *intrinsic absorption coefficient* μ_i)[19] in Fig. 3(c). Indeed, for SiNCs with diameter bigger than about 3 nm, all μ_i spectra are almost equal. However, for smaller NCs, μ_i values are reduced in accord with the PL-based method (Fig. 3(a)).

In Fig. 3(a), we compare results of the PL-modulation technique with ACS values obtained by absorption at 405 nm (i.e., the excitation laser wavelength). The PL emission wavelength is converted into NC diameter using calculation by Luo, Stradins, and Zunger.[20] Then, absorption-derived ACS values are plotted (open symbols) at the position of the size-distribution peak and the color rectangles indicate the half-peak width of the distribution. For samples W3 and W4, the real size distributions (published in Ref. 6) are taken and perfect agreement of ACS from both methods is obtained, while for W1 and W2 we have to use estimated values and rough agreement of ACS values is observed.

This unique comparison of the two independent methods reveals the important role of a NC-size distribution. One significant advantage of the PL method is its size-selectivity achieved by limiting the detection range (we used a bandwidth of 5 nm, which correspond to 5–18 meV band in the investigated spectral range). On the other hand, the absorption technique is simpler and straightforward but probes the whole ensemble of size-distributed NCs and relies on the knowledge of a NC density and size-distribution.

In principle, the two methods may reveal different values of ACS as one approach is related to extinction and the other to PL-excitation. For example, a strong PL QY

size-dependence or efficient energy transfer (from small to big NCs) can cause deviation of ACS determined by the two methods. Indeed, in our SRON ML samples, we observe a peak of PL QY for Si NCs with diameter of about 4 nm and considerable decrease toward smaller or bigger NCs (similar to the report by Ledoux *et al.*[21]) which may cause slightly higher ACS values derived from PL in samples W1 and W2. Possible exciton migration effects[22] may be neglected here as our previous studies[23] show that at low electric field the migration is limited to the trapping of carriers in neighboring defects. Such loss of excitons in the non-radiative centers is intrinsically included in the differential equations (Eqs. (1)–(3)) as the non-radiative term of the effective lifetime τ_{PL}.

In conclusions, we have studied and analyzed the method of ACS measurement via the power-dependent PL-kinetics in SiNCs. The limits of its application and the key points for its implementation are defined. The direct comparison of ACS values obtained by the PL technique and the independent absorption method give consistent results around 10^{-15} cm^2 for SiNCs with mean diameters between 3 and 5 nm. For smaller NCs, the ACS value decreases but still giving roughly comparable values by the two methods. The described methods and derived conclusions have general validity for nanocrystalline ensembles independently of their material composition (group IV, II–VI, and III–V semiconductors).

This work was financially supported by the EU-project NASCEnT (FP7-245977). The Prague group acknowledges support within the framework of the Czech-Japan collaborative Project LH14246 (MSMT CR).

[1]D. V. Talapin, J. S. Lee, M. V. Kovalenko, and E. V. Shevchenko, Chem. Rev. **110**, 389 (2010).
[2]*Nanotechnology and Photovoltaic Devices*, edited by J. Valenta and S. Mirabella (Pan Stanford Publishing, Singapore, 2015).
[3]E. Petryayeva, W. R. Algar, and I. R. Medintz, Appl. Spectrosc. **67**, 215 (2013).
[4]P. Yu, M. C. Beard, R. J. Ellingson, S. Ferrere, C. Curtis, J. Drexler, F. Luiszer, and A. J. Nozik, J. Phys. Chem. B **109**, 7084 (2005).
[5]A. M. Hartel, D. Hiller, S. Gutsch, P. Löper, S. Estradé, F. Peiró, B. Garrido, and M. Zacharias, Thin Solid Films **520**, 121 (2011).
[6]S. Gutsch, D. Hiller, J. Laube, M. Zacharias, and C. Kübel, Beilstein J. Nanotechnol. **6**, 964 (2015).
[7]Z. Remeš, R. Vasudevan, K. Jarolimek, A. H. M. Smets, and M. Zeman, Solid State Phenom. **213**, 19 (2014).
[8]J. Valenta and M. Greben, AIP Adv. **5**, 047131 (2015).
[9]M. T. Trinh, R. Limpens, and T. Gregorkiewicz, J. Phys. Chem. C **117**, 5963 (2013).
[10]D. Kovalev, J. Diener, H. Heckler, G. Polisski, N. Künzner, and F. Koch, Phys. Rev. B **61**, 4485 (2000).
[11]P. Hapala, K. Kusova, I. Pelant, and I. Jelinek, Phys. Rev. B **87**, 195420 (2013).
[12]I. Pelant and J. Valenta, *Luminescence Spectroscopy of Semiconductors* (Oxford University Press, 2012).
[13]C. Garcia, B. Garrido, P. Pellegrino, R. Ferre, J. A. Moreno, J. R. Morante, L. Pavesi, and M. Cazzanelli, Appl. Phys. Lett. **82**, 1595 (2003).
[14]J. Linnros, N. Lalic, A. Galeckas, and V. Grivickas, J. Appl. Phys. **86**, 6128 (1999).
[15]G. S. Higashi and M. A. Kastner, Philos. Mag. B **47**, 83 (1983).
[16]A. M. Hartel, S. Gutsch, D. Hiller, and M. Zacharias, Phys. Rev. B **87**, 035428 (2013).
[17]C. Meier, A. Gondorf, S. Lüttjohann, A. Lorke, and H. Wiggers, J. Appl. Phys. **101**, 103112 (2007).
[18]See http://goldbook.iupac.org/A00028.html for IUPAC Gold Book.
[19]Z. Hens and I. Moreels, J. Mater. Chem. **22**, 10406 (2012).
[20]J.-W. Luo, P. Stradins, and A. Zunger, Energy Environ. Sci. **4**, 2546 (2011).
[21]G. Ledoux, J. Gong, F. Huisken, O. Guillois, and C. Reynaud, Appl. Phys. Lett. **80**, 4834 (2002).
[22]F. Priolo, G. Franzo, D. Pacifici, V. Vinciguerra, F. Iacona, and A. Irrera, J. Appl. Phys. **89**, 264 (2001).
[23]S. Gutsch, J. Laube, A. M. Hartel, D. Hiller, N. Zakharov, P. Werner, and M. Zacharias, J. Appl. Phys. **113**, 133703 (2013).